# Measurement of the molecular content of binary nuclei. III. Use of the nucleation rate surfaces for the water-n-alcohol series

R. Strey, Y. Viisanen, and P. E. Wagner

Citation: The Journal of Chemical Physics **103**, 4333 (1995); doi: 10.1063/1.470672
View online: http://dx.doi.org/10.1063/1.470672
View Table of Contents: http://scitation.aip.org/content/aip/journal/jcp/103/10?ver=pdfcov
Published by the AIP Publishing





# Measurement of the molecular content of binary nuclei. III. Use of the nucleation rate surfaces for the water-*n*-alcohol series

R. Strey,[a] Y. Viisanen,[b] and P. E. Wagner[c]
*Max-Planck-Institut für Biophysikalische Chemie, Postfach 2841, D-37018 Göttingen, Germany*

(Received 8 March 1995; accepted 6 June 1995)

In two preceding papers the molecular content of binary ethanol-hexanol and water-ethanol nuclei, respectively, was determined from nucleation rate measurements. While nucleation of ethanol-hexanol mixtures behaved nearly ideal, a strong mutual nucleation enhancement for water-ethanol was observed. Here we extend the investigations to include the longer chain alcohols, that is water $-C_iH_{2i+1}OH$ systems with $i=2$ to 6. Using the nucleation pulse technique developed in the past few years nucleation rates in the range $10^5<J/cm^{-3}\,s^{-1}<10^9$ are measured. Ranging from pure water to pure alcohol the water and alcohol activities, $a_1$ and $a_2$, respectively, are varied for each system with about ten intermediate compositions at constant temperature $T=260$ K. Aside from a remarkably similar behavior of the various alcohols, one observes that with increasing alcohol chain length the mutual nucleation enhancement decreases. Since all water-alcohol systems behave qualitatively similar, we confine ourselves to present the full experimental nucleation rate surface $J(a_1,a_2)$ for one system, water-*n*-pentanol, as an example. From the nucleation rate surface for each system the onset activities corresponding to a reference nucleation rate of $J_0=10^7$ $cm^{-3}\,s^{-1}$ are determined. From the slopes of the nucleation rate surfaces one obtains the individual numbers of molecules in the critical cluster $n_i^*$ because $\partial \ln J/\partial \ln a_i \approx n_i^*$. As noted previously, determining the molecular content this way does not involve any particular theoretical model, nor does it depend on the structure of the critical cluster. Accordingly, the average composition of the critical clusters can be obtained. An alcohol enrichment of the nuclei at low alcohol activity fraction is found for all alcohols examined, the degree diminishing with increasing alcohol chain length. The appearance of a macroscopic miscibility gap for the higher alcohols is not reflected in any qualitative change of the composition of the microscopic nuclei. © *1995 American Institute of Physics.*

## I. INTRODUCTION

Gas to liquid phase transitions involving several condensable species occur in various environmentally and technologically relevant situations. Particularly meteorological processes are strongly influenced by simultaneous condensation of water vapor and various trace gases in the atmosphere. The formation of fog and cloud droplets has received considerable attention in recent years because of possible implications in connection with the evolution of the global climate.[1]

Vapor condensation is usually preceded by the formation of transient clusters of the condensed phase. In the absence of aerosol particles or other nucleation agents providing substrates for condensation particle nucleation can occur by spontaneous cluster formation.[2] In unary (single-component) vapors this homogeneous nucleation process generally requires considerable vapor supersaturations, which are rarely observed in practical situations. Homogeneous nucleation in vapor mixtures, however, often occurs at much lower supersaturations. Accordingly, heteromolecular homogeneous nucleation is considered as an important process also for the atmosphere.[3]

The first theoretical description of homogeneous nucleation has been based on a macroscopic drop model.[4] Becker and Döring[5] developed the so-called classical nucleation theory for unary vapors, which was generalized to binary systems by Volmer[6,7] and Reiss.[8] A study by Doyle[9] on binary homogeneous nucleation has subsequently led to considerable controversy.[9–16] The general description of the structure of binary clusters is difficult, particularly for nonideal systems, where inhomogeneous distribution and orientation of the molecules and possibly surface enrichment can be expected. This has led several authors to consider explicit cluster models.[17–19]

The macroscopic drop models are based on idealizing assumptions, which may not be fulfilled for the critical clusters consisting of 10 to 100 molecules. A treatment based on microscopic molecular models might account for the detailed structure of the clusters. Various cluster definitions have been suggested.[20–22] However, insufficient knowledge of the intermolecular potentials for interesting molecules has so far precluded quantitative predictions for relevant systems. Recently progress has come from the density functional approach.[23,24] Similar deviations from classical nucleation theory as found in experimental studies were observed for selected simple atoms.

The above-mentioned theoretical models for heteromolecular homogeneous nucleation in binary vapors are based on the assumption that nucleation proceeds through the formation of mixed critical clusters with a certain well-defined composition. This assumption, however, may not be valid for

[a]To whom correspondence should be addressed.
[b]Finnish Meteorological Institute, Sahaajankatu 22E, SF-008100 Helsinki, Finland.
[c]Institut für Experimentalphysik, Universität Wien, Boltzmanngasse 5, A-1090 Wien, Austria.

mixtures of molecules only partially miscible in liquid state. Little is known so far about the binary homogeneous nucleation of partially miscible liquids. Ray *et al.*[25] have theoretically examined the case of simultaneous occurrence of two types of critical clusters with correspondingly different compositions.

In the present paper we report nucleation pulse measurements of nucleation rates in supersaturated water-*n*-alcohol vapor mixtures. While for the nucleation conditions considered water-ethanol and water-*n*-propanol are still fully miscible in the liquid state, the binary systems of water and the higher *n*-alcohols exhibit an increasingly larger miscibility gap. Accordingly, a systematic study of homogeneous nucleation for the homologous series of the water-*n*-alcohol vapor mixtures can provide informations on the dependence of the binary homogeneous nucleation process on the miscibility of the condensing liquids. As will be shown below, the way the nucleation rate measurements are performed allows general conclusions regarding size and composition of the corresponding critical clusters without reference to any specific nucleation theory.[26–31] Thereby the nonideal composition of the critical clusters forming in various water-*n*-alcohol vapor mixtures considered can be characterized quantitatively.

The experimentation and evaluation procedures described in this paper can be applied to a variety of carrier gases and vapor mixtures. The present study can actually serve as a starting point for investigations concerning atmospherically relevant systems.

In the next section the experimental procedure is described pertinent to the systems studied here. Further details have been described in preceding papers I and II[29,30] and a recent feature article describing the nucleation pulse method.[52] The full set of nucleation rate data for the water-*n*-pentanol system is presented here along with the evaluation procedure. The same procedure has been applied to the other water-*n*-alcohol systems. Comparisons are performed which allow similarities and differences of the various systems to be discussed.

## II. EXPERIMENT

Experiments on homogeneous nucleation in supersaturated vapors are frequently performed in three steps. At first, particle free vapors or vapor mixtures with well-defined partial vapor pressures are prepared. Secondly, vapor supersaturations required for significant nucleation to occur are generated. In the third step the subsequent nucleation process is detected. As direct observation of the nucleation process is impossible in most cases, actually the droplets growing subsequent to the formation of critical clusters are usually monitored and counted.

Supersaturated vapor mixtures can be generated by nonisothermal diffusion currents as occurring in static[32–36] or steady-state flow[37] diffusion chambers, by adiabatic expansions obtained using expansion chambers,[28–30,39–48,52] shock tubes[49] or supersonic nozzles,[50,51] or by turbulent mixing of two gas flows at different temperatures.[38] Frequently the vapor mixtures considered are obtained by evaporation from liquid mixtures with properly chosen compositions. This procedure, however, can practically only be used for the study of binary nucleation of fully miscible liquids and is not applicable for the present study.

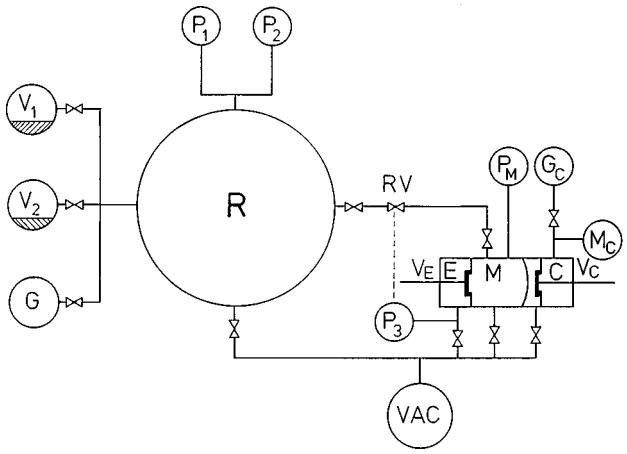


FIG. 1. Schematic diagram showing vapor generation system and expansion chamber. The vapor generation system consists of vaporizers $V_1$ and $V_2$, carrier gas bottle $G$ and mixing receptacle $R$. The expansion chamber is divided into measuring section $M$, expansion volume $E$ and compression volume $C$. Connections to a vacuum system are provided.

In order to allow a unique interpretation of the experimental data obtained and a quantitative determination of nucleation rates, it is advantageous to observe the nucleation process in steady state. This requires that the nucleation process is decoupled from subsequent condensational growth of the new phase thereby avoiding a self-quenching of the nucleation process. Decoupling of nucleation and condensational growth can be achieved by removing the growing particles from the sensing volume at a sufficiently high rate. This procedure is usually applied in diffusion chambers. Furthermore, nucleation and growth can be decoupled by deliberately terminating the nucleation process after a sufficiently short time interval before substantial condensational drop growth has occurred and thus considering a nucleation pulse.[52]

### A. Experimental arrangement

In this paper we are presenting results of an expansion chamber study of homogeneous nucleation in binary vapor mixtures based on the nucleation pulse method. A detailed description of the experimental system has been given elsewhere,[52] here we are summarizing those features particularly relevant for the present experiments. In order to allow the generation of vapor mixtures regardless of the miscibility of the corresponding liquids, the vapors are obtained from two separate vaporizers. Each vaporizer contains one of the *pure* liquids considered. As illustrated in Fig. 1, the vaporizers $V_1$ and $V_2$ as well as a bottle $G$ containing compressed inert gas are separately connected to a thermostated mixing plenum $R$ (volume about 5000 $cm^3$) via precision metering valves.

For measurement of the gas pressure inside $R$ precision pressure transducers $P_1$ and $P_2$ (full scale ranges of order 1 MPa and 1 kPa, respectively), are provided. The vapor supply unit, consisting of vaporizers $V_1$ and $V_2$, mixing recep-

tacle $R$, pressure transducers $P_1$ and $P_2$, corresponding valve manifold and connecting stainless steel tubes, is placed inside a heated temperature controlled box in order to prevent premature condensation of the vapors considered. Via the electronically controlled regulation valve $RV$ and a thermostated stainless-steel tube the mixing plenum $R$ is connected to a cylindrical expansion chamber. The thermostated expansion chamber has essentially three partitions, the actual measuring chamber $M$ (volume about 25 $cm^3$), the low-pressure expansion volume $E$ and the high-pressure compression volume $C$. Connections between these partitions are provided via the fast-action valves $V_E$ and $V_C$, respectively, which are controlled by a specially designed trigger system (reproducibility better than 50 $\mu$s). Via proper valve and regulation manifolds the high-pressure compression volume $C$ is connected to a bottle $G_C$ containing compressed inert gas, while measuring chamber $M$ and low-pressure expansion volume $E$ as well as the mixing plenum $R$ are connected to a vacuum system VAC. Absolute gas pressures in measuring chamber $M$ and expansion volume $E$ can be measured by the precision pressure transducer $P_3$ (full scale range about 150 kPa), the pressure in the compression volume $C$ can be determined by the manometer $M_C$. The piezoelectric pressure transducer $P_M$ (rise time about 5 $\mu$s) is provided for quantitatively monitoring the pressure changes inside the measuring chamber $M$ during the actual nucleation measurement period. In order to avoid contamination, the measuring chamber $M$ is separated from the compression volume $C$ by means of a flexible but impermeable Teflon membrane.

The actual vapor mixture considered during a series of measurements is first prepared in the mixing receptacle $R$ (see Fig. 1). Before each single experimental run a certain amount of this vapor mixture is passed into the measuring volume $M$ of the expansion chamber. Measurements of homogeneous nucleation rates in supersaturated vapors are performed using the nucleation pulse method.[52] Nucleation pulses in the measuring volume are then generated by expansion and recompression in a well-defined time sequence, the pressure ratios being kept constant during each series of measurements. The condensation process occurring inside the measuring volume $M$ subsequent to nucleation is monitored by a light scattering method.

### B. Measurement of vapor phase activities

Before starting a series of experiments, the various parts of the measuring system are evacuated to a few $10^{-4}$ Pa. The temperature of the expansion chamber is set to the desired value $T_0$, which is kept constant to within $10^{-2}$ K during the whole series of measurements. The mixing plenum $R$ is thermostated with the same precision in order to ensure well-defined conditions during the filling procedure. The vaporizers $V_1$ and $V_2$ are kept at a somewhat higher temperature and the temperature of the box containing the whole vapor supply unit is chosen sufficiently above these temperatures in order to prevent vapor condensation in any part of the vapor generation system. After sufficient evacuation a proper amount of each of the two *pure* liquids considered in a particular experimental series is passed into the respective vaporizer. A number of subsequent evacuation steps are then performed in order to quantitatively remove any gases dissolved in the liquids.

Next the desired vapor-gas mixture with partial vapor pressures $p_{V1}^{(R)}$ and $p_{V2}^{(R)}$ and partial carrier gas pressure $p_G^{(R)}$ is prepared in the mixing receptacle $R$. To this end the two vapors considered and the carrier gas are sequentially passed into the mixing receptacle via precision metering valves. Periods of at least 15 in are allowed for proper equilibration of the inside walls of the mixing receptacle $R$. The components are admitted to the plenum $R$ in the sequence of increasing partial pressures. Measurements of the total pressure by means of the pressure transducers $P_1$ and $P_2$ during and after each filling step allow direct quantitative setting of the various partial pressures in the mixing receptable $R$ independent of equilibrium vapor pressure data for the compounds considered. As a result the vapor fractions

$$\omega_i=\frac{p_{Vi}^{(R)}}{p_{V1}^{(R)}+p_{V2}^{(R)}+p_G^{(R)}}=\frac{p_{Vi}^{(R)}}{p_{TOT}^{(R)}}, \quad (i=1,2) \tag{1}$$

of both vapor components in the vapor-carrier gas mixture are quantitatively determined. During the filling procedure care must be taken to keep the vapor mixture undersaturated with respect to the temperature of the mixing receptacle $R$ in order to avoid condensation inside $R$.

Before each measuring run the compression valve $V_C$ is closed, the pressure in the compression volume $C$ is set to the desired value and the Teflon membrane is moved to a defined starting position by evacuation of the partition between Teflon membrane and compression valve $V_C$. Then at least three measuring chamber volumes of the vapor-carrier gas mixture are passed from the mixing receptacle $R$ through the measuring chamber $M$ and the open expansion valve $V_E$. During this flushing period the total pressure inside the measuring chamber $M$ is measured by the pressure transducer $P_3$ and kept at a selectable *constant* value $p_0$ by means of the electronically regulated needle valve $RV$. This procedure is essential for establishing the required equilibrium conditions at the inside walls of the measuring chamber $M$. It turned out that reproducible experiments could only be performed after proper equilibration of the chamber walls. After closing the expansion valve $V_E$ finally the pressure in the expansion volume $E$ is set to the desired value.

At the beginning of an actual nucleation experiment $V_E$ is opened thereby initializing an adiabatic expansion process inside the measuring chamber $M$ and subsequently homogeneous nucleation starts. The expanded supersaturated state, during which nucleation occurs, is maintained for typically 1 ms. Opening of $V_C$ then causes a slight adiabatic recompression inside the measuring chamber $M$ practically terminating the nucleation process. The pressure changes occurring inside the measuring chamber $M$ during the nucleation experiment are monitored by the piezoelectric pressure transducer $P_M$. Expansion pulses with very nearly flat pulse plateaus are observed. As described in detail elsewhere,[52] the plateau value $\Delta p_{\exp t}$ of the pressure drop as well as the duration $\Delta t_{\exp t}$ of the pulse plateau are evaluated from the experimental pressure signal. Since the initial total pressure $p_0$ in the

measuring chamber $M$ has been set and measured before expansion, the average pressure expansion ratio

$$\beta = \frac{p_0 - \Delta p_{\exp t}}{p_0} \tag{2}$$

during the nucleation pulse is obtained. Thus taking into account the constant value $T_0$ of the chamber temperature, the average nucleation temperature

$$T_{\exp t} = T_0 \beta^{1-1/\kappa} \tag{3}$$

occurring during the nucleation pulse can be calculated. The ratio $\kappa$ of the specific heats of the carrier gas-vapor mixture is determined according to Richarz.[53] It should be noted that during one measurement series the vapor fractions $\omega_1$ and $\omega_2$ and thus $\kappa$ remain unchanged. As the chamber temperature $T_0$ is fixed and $\Delta p_{\exp t}/p_0$ and thus $\beta$ are kept at the same value, a constant nucleation temperature $T_{\exp t}$ is achieved during one series of experiments within a few $10^{-2}$ K. In fact, all measurements reported in the present paper were performed at the same nucleation temperature of 260 K. As the vapor fractions $\omega_1$ and $\omega_2$ will not change during expansion, the actual partial vapor pressures

$$p_{Vi,\exp t} = \beta \omega_i p_0, \quad (i=1,2), \tag{4}$$

during nucleation inside the measuring chamber $M$ are obtained from directly measurable quantities and without reference to literature data on the compounds considered. Now using data on the equilibrium vapor pressures $p^0_{V1,e}(T)$ and $p^0_{V2,e}(T)$ over the *pure* liquids considered, the vapor phase activities

$$a_{i,\exp t} = \frac{p_{Vi,\exp t}}{p^0_{Vi,e}(T_{\exp t})} = \frac{\beta \omega_i}{p^0_{Vi,e}(T_{\exp t})}\, p_0, \quad (i=1,2) \tag{5}$$

can be calculated. As $\beta$, $\omega_i$, and $T_{\exp t}$ remain unchanged during one measurement series, the vapor phase activities $a_{1,\exp t}$ and $a_{2,\exp t}$ are simply selected by proper setting of the initial total pressure $p_0$ inside the measuring chamber $M$. The ratio of the two vapor phase activities is determined by the composition of the vapor-carrier gas mixture and therefore remains constant during one measurement series. It should be noted that vapor phase activity and supersaturation are identical for unary vapors. However, these quantities have to be carefully distinguished for the case of vapor mixtures.

### C. Measurement of nucleation rates

For detection of the nucleation process the condensational droplet growth subsequent to nucleation is observed. To this end the growing droplets are illuminated by a laser beam, while a photodiode monitors the light flux transmitted through the measuring chamber and a photomultiplier measuring the light flux scattered at a constant forward scattering angle of 15°. At the intersection of the incident laser beam and the observation cone of the scattered light photomultiplier a comparatively small scattering volume in the center of the measuring chamber $M$ is defined, where the nucleation process is actually detected.

While practically no new droplets are formed after recompression, the droplets formed during the nucleation pulse continue to grow by condensation of the still supersaturated vapor mixture. The number concentration $C_{\exp t}$ of the growing droplets is determined by the constant angle Mie scattering (CAMS) method.[54] As described in detail elsewhere,[52] simultaneous monitoring of scattered and transmitted laser light fluxes and comparison to Lorenz–Mie theory[55,56] allow absolute determination of the number concentration of growing spherical droplets at various times during the growth process. No external reference standards are required. Assuming that each individual growing droplet corresponds to just one nucleation event and that nucleation proceeds nearly in steady state during the nucleation pulse,[57] the nucleation rate occurring in the measuring chamber can now be determined as

$$J_{\exp t} = \frac{C_{\exp t}}{\Delta t_{\exp t}}. \tag{6}$$

The droplet number concentrations $C_{\exp t}$ are typically measured already several ms after nucleation has occurred, when droplets have grown to about 0.7 $\mu$m in radius. The present experimental system allows to measure nucleation rates ranging from about $10^5$ to $10^9$ $\mathrm{cm}^{-3}\,\mathrm{s}^{-1}$. While the lower limit of the measuring range is related to the minimum number of droplets required inside the sensing volume of the light scattering arrangement, the finite amount of the vapors available for condensation restricts the size of the condensing droplets and accordingly concentrations cannot be determined beyond a certain upper limit. It is notable that the CAMS method allows time-resolved droplet growth measurements.[58,59] By means of the CAMS measurements it can therefore be verified that nucleation and condensational droplet growth are actually decoupled to a large extent in the present experiments. Furthermore influences due to heterogeneous nucleation in the measuring chamber $M$ can safely be detected by means of the CAMS method.[52]

According to the above described measurement procedure the nucleation pulse system used in the present study is characterized by the following features: (1) The partial vapor pressures and the temperature are uniform inside the sensing volume. (2) The partial vapor pressures and the temperature are practically constant during the period of nucleation. (3) Partial vapor pressures and temperature during nucleation can be calculated in a direct way referring only to data on the ratios of specific heats of the compounds considered. (4) The nucleation temperature can be selected independent of the partial vapor pressures thus allowing to obtain isothermal data sets. (5) Vapor mixtures can be generated regardless of the miscibility of the condensing liquids. (6) Nucleation and growth are practically decoupled and steady-state nucleation conditions are achieved. (7) The observation process has negligible influence on the nucleation in the measuring chamber. (8) Heterogeneous nucleation can be experimentally discriminated from homogeneous nucleation. (9) Measurement of nucleation rates can be performed quantitatively over ranges of vapor phase activities rather than just determination of nucleation onset conditions.

## III. RESULTS

Homogeneous nucleation has been studied for five different binary water-*n*-alcohol vapor mixtures. Nucleation rates were measured over ranges of vapor phase activities at the constant temperature of 260 K. Argon was used as the carrier gas. As will be shown below, the nucleation of the various systems considered exhibits significant differences as the alkyl chain length of the alcohols is varied from 2 to 6 carbon atoms. However, a similar general behavior was found. Therefore it is sufficient to describe the actual experimental data for one selected system. In order to illustrate the results obtained, the water-*n*-pentanol system will be discussed in some detail below.

### A. The nucleation rate surface

The experimental system described in the preceding sections, allows to measure the nucleation rate $J$ as function of the vapor phase activities $a_1$ and $a_2$ of water and alcohol vapors, respectively. Since the vapor mixtures are prepared in the receptacle $R$, the ratio $a_2/a_1$ of the two activities remains constant during each series of experiments while the total pressure and thus the activities are changed. Therefore it is useful to consider the experimental nucleation rates as functions of the activity fraction

$$x=\frac{a_2}{a_1+a_2} \tag{7}$$

of the alcohol considered and of the variable

$$a=\sqrt{a_1^2+a_2^2}. \tag{8}$$

During each individual experimental series performed $x$ remains constant while $a$ is varied according to changes of $a_1$ and $a_2$.

In Fig. 2 the experimental nucleation rates are plotted versus $a$. The data display a systematic variation with the activity fraction $x$ of *n*-pentanol. It can be seen that the ln $J$ versus $a$ representation of the datapoints is quite linear. The solid lines indicate linear least-squares fits to the data which allow to accurately determine the slopes $\partial \ln J/\partial a$ at fixed activity fraction $x$. As one starts with pure water [Fig. 2(a)] the slope of the curves increases with increasing $x$ while the curves are moved to smaller $a$. As $x$ becomes larger than 0.5 the trend reverses until one finally arrives at pure *n*-pentanol [Fig. 2(b)]. Concomitantly, the slope of the curves decreases with increasing $a$. The actual numerical values and the experimental measurables are presented in Table I.

As shown previously[60] and described in detail in the experimental sections of the preceding papers I and II,[29,30] the individual nucleation rate curves measured for various constant ratios $a_2/a_1$ determine a nucleation rate surface in the ln $J$-$a_1$-$a_2$ space. A three-dimensional presentation of the individual ln $J$ versus $a$ curves for water-*n*-pentanol at 260 K is shown in Fig. 3.

As can be seen from Fig. 3, the experimental data of the individual ln $J$ versus $a$ curves indeed shape a surface in the ln $J$-$a_1$-$a_2$ space.

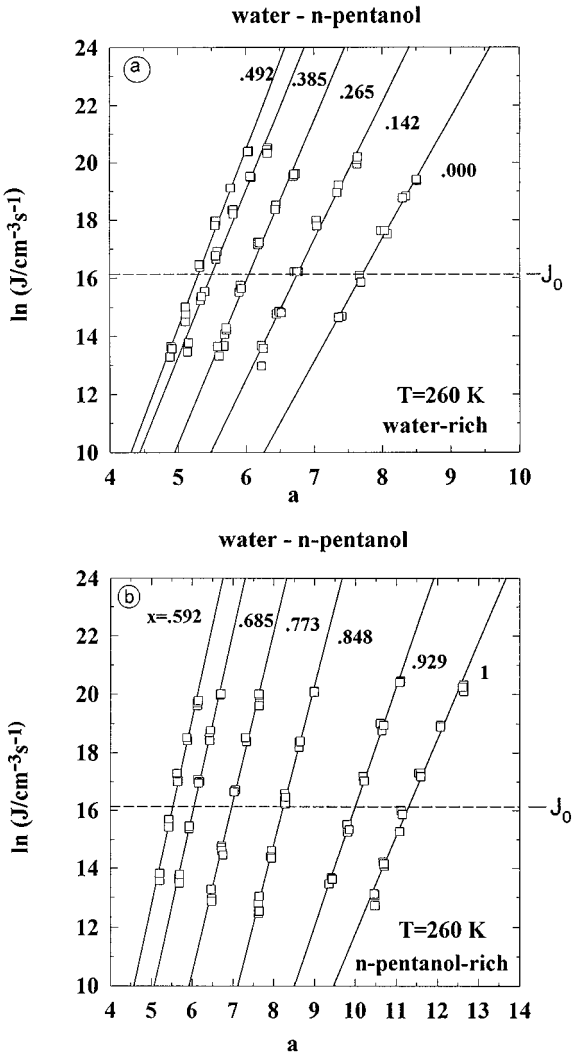


FIG. 2. Experimental nucleation rates for the water-*n*-pentanol system shown as a function of $a$, where $a=\sqrt{a_1^2+a_2^2}$ and $a_1$ and $a_2$ are the water and alcohol activity, respectively. Note the trend reversal near an activity fraction $x=0.5$, where $x=a_2/(a_1+a_2)$. The full lines are linear least squares fits providing $\partial \ln J/\partial a$. The dashed line indicates the reference nucleation rate $J_0$.

### B. Determination of onset activities

In Fig. 3 the intersection of this surface with an $a_1$-$a_2$ plane corresponding to a fixed nucleation rate $J_0=10^7$ cm$^{-3}$ s$^{-1}$ is indicated by the dotted line in this plane. The rate $J_0=10^7$ cm$^{-3}$ s$^{-1}$ actually represents the center of our measuring range and thus determination of the activities $a_{10}$ and $a_{20}$ corresponding to this nucleation rate $J_0$ is particularly accurate. In the following we will refer to $a_{10}$ and $a_{20}$ as *onset activities* corresponding to the *reference nucleation rate* $J_0$:

$$J(a_{10},a_{20},T)=J_0. \tag{9}$$

The onset activities corresponding to the reference nucleation rate $J_0=10^7$ cm$^{-3}$ s$^{-1}$ are indicated by the full circles on the dotted line in the $a_1$-$a_2$ plane in Fig. 3. It should be mentioned that onset activities corresponding to a reference nucleation rate of 1 cm$^{-3}$ s$^{-1}$ have sometimes been termed ''critical'' activities.

TABLE I. Results of the nucleation rate measurements for water-*n*-pentanol. Experimental measurables: Initial chamber temperature $T_0$ (in °C), vapor fractions in the vapor-carrier gas mixture $\omega_i$ (in %), activity fraction of *n*-pentanol in the vapor mixture $x$, initial total pressure $p_0$ (in kPa). $\Delta p$ is the measured difference between $p_0$ and the actual pressure $p_{\exp t}$ during the nucleation pulse. $J_{\exp t}$ (in $\mathrm{cm}^{-3}\,\mathrm{s}^{-1}$) is the experimental nucleation rate. The average temperature $T_{\exp t}$ (in K) and the average vapor phase activities $a_i$ during the nucleation pulse are calculated using Poisson's equation [Eq. (3)].

A. $T_0=32.25$ °C $\omega_1=2.2684\%$ $\omega_2=0\%$ $x=0$

| $p_0$ | $\Delta p/p_0$ | $J_{\exp t}$ | $T_{\exp t}$ | $a_1$ | $a_2$ |
|---|---|---|---|---|---|
| 122.67 | 0.3347 | 2.6e8 | 260.01 | 8.51 | 0 |
| 122.67 | 0.3347 | 2.6e8 | 260.03 | 8.51 | 0 |
| 122.67 | 0.3346 | 2.7e8 | 260.03 | 8.50 | 0 |
| 120.22 | 0.3348 | 1.5e8 | 260.01 | 8.35 | 0 |
| 120.22 | 0.3343 | 1.4e8 | 260.08 | 8.30 | 0 |
| 115.46 | 0.3355 | 4.0e7 | 259.89 | 8.08 | 0 |
| 115.46 | 0.3344 | 4.5e7 | 260.07 | 7.98 | 0 |
| 115.46 | 0.3350 | 4.5e7 | 259.97 | 8.04 | 0 |
| 110.89 | 0.3344 | 9.7e6 | 260.07 | 7.67 | 0 |
| 110.89 | 0.3346 | 7.7e6 | 260.03 | 7.69 | 0 |
| 106.50 | 0.3350 | 2.4e6 | 259.97 | 7.41 | 0 |
| 106.50 | 0.3344 | 2.3e6 | 260.07 | 7.36 | 0 |

B. $T_0=32.30$ °C $\omega_1=2.0485\%$ $\omega_2=0.01489\%$ $x=0.142$

| $p_0$ | $\Delta p/p_0$ | $J_{\exp t}$ | $T_{\exp t}$ | $a_1$ | $a_2$ |
|---|---|---|---|---|---|
| 120.22 | 0.3350 | 4.6e8 | 259.99 | 7.53 | 1.25 |
| 120.22 | 0.3349 | 5.4e8 | 259.99 | 7.53 | 1.25 |
| 120.22 | 0.3351 | 5.9e8 | 259.97 | 7.54 | 1.25 |
| 115.46 | 0.3352 | 2.2e8 | 259.95 | 7.26 | 1.21 |
| 115.46 | 0.3350 | 1.7e8 | 259.98 | 7.24 | 1.20 |
| 115.46 | 0.3351 | 1.7e8 | 259.97 | 7.24 | 1.20 |
| 110.89 | 0.3349 | 6.5e7 | 260.00 | 6.94 | 1.15 |
| 110.89 | 0.3351 | 5.3e7 | 259.97 | 6.95 | 1.15 |
| 106.50 | 0.3343 | 1.1e7 | 260.09 | 6.62 | 1.10 |
| 106.50 | 0.3351 | 1.1e7 | 259.96 | 6.68 | 1.11 |
| 106.50 | 0.3348 | 1.1e7 | 260.02 | 6.66 | 1.10 |
| 102.28 | 0.3344 | 2.6e6 | 260.08 | 6.36 | 1.05 |
| 102.28 | 0.3349 | 2.8e6 | 260.00 | 6.40 | 1.06 |
| 102.28 | 0.3353 | 2.7e6 | 259.94 | 6.43 | 1.07 |
| 98.23 | 0.3348 | 8.7e5 | 260.01 | 6.14 | 1.02 |
| 98.23 | 0.3348 | 4.3e5 | 260.02 | 6.14 | 1.02 |
| 98.23 | 0.3351 | 7.9e5 | 259.96 | 6.17 | 1.02 |

C. $T_0=32.34$ °C $\omega_1=1.7550\%$ $\omega_2=0.02769\%$ $x=0.265$

| $p_0$ | $\Delta p/p_0$ | $J_{\exp t}$ | $T_{\exp t}$ | $a_1$ | $a_2$ |
|---|---|---|---|---|---|
| 117.82 | 0.3351 | 3.3e8 | 259.95 | 6.33 | 2.28 |
| 117.82 | 0.3348 | 3.0e8 | 260.00 | 6.30 | 2.27 |
| 117.82 | 0.3349 | 3.2e8 | 259.98 | 6.31 | 2.27 |
| 113.15 | 0.3349 | 1.1e8 | 259.98 | 6.06 | 2.18 |
| 113.15 | 0.3347 | 9.5e7 | 260.01 | 6.05 | 2.18 |
| 108.67 | 0.3348 | 3.0e7 | 260.00 | 5.81 | 2.09 |
| 108.67 | 0.3348 | 2.8e7 | 260.00 | 5.81 | 2.09 |
| 108.67 | 0.3350 | 3.0e7 | 259.97 | 5.83 | 2.10 |
| 104.37 | 0.3343 | 5.5e6 | 260.08 | 5.55 | 1.99 |
| 104.37 | 0.3346 | 6.9e6 | 260.03 | 5.57 | 2.00 |
| 104.37 | 0.3348 | 6.2e6 | 259.99 | 5.58 | 2.01 |
| 100.24 | 0.3345 | 8.5e5 | 260.05 | 5.34 | 1.92 |
| 100.24 | 0.3344 | 8.7e5 | 260.05 | 5.34 | 1.92 |
| 100.24 | 0.3345 | 1.3e6 | 260.04 | 5.35 | 1.92 |
| 100.24 | 0.3350 | 1.5e6 | 259.97 | 5.37 | 1.94 |
| 100.24 | 0.3349 | 1.6e6 | 259.98 | 5.37 | 1.93 |
| 98.24 | 0.3350 | 6.1e5 | 259.97 | 5.27 | 1.90 |
| 98.24 | 0.3347 | 8.5e5 | 260.02 | 5.25 | 1.89 |

D. $T_0=32.40$ °C $\omega_1=1.5226\%$ $\omega_2=0.04168\%$ $x=0.385$

| $p_0$ | $\Delta p/p_0$ | $J_{\exp t}$ | $T_{\exp t}$ | $a_1$ | $a_2$ |
|---|---|---|---|---|---|
| 115.46 | 0.3350 | 8.0e8 | 259.97 | 5.36 | 3.35 |
| 115.46 | 0.3349 | 7.5e8 | 260.00 | 5.35 | 3.34 |

TABLE I. (*Continued*.)

D. $T_0=32.40$ °C $\omega_1=1.5226\%$ $\omega_2=0.04168\%$ $x=0.385$

| | | | | | |
|---|---|---|---|---|---|
| 115.46 | 0.3350 | 6.7e8 | 259.98 | 5.35 | 3.35 |
| 110.89 | 0.3352 | 2.9e8 | 259.95 | 5.15 | 3.22 |
| 110.89 | 0.3350 | 3.0e8 | 259.98 | 5.14 | 3.21 |
| 106.50 | 0.3346 | 9.3e7 | 260.04 | 4.92 | 3.07 |
| 106.50 | 0.3348 | 9.4e7 | 260.01 | 4.93 | 3.08 |
| 106.50 | 0.3348 | 8.1e7 | 260.02 | 4.93 | 3.08 |
| 102.28 | 0.3347 | 2.2e7 | 260.03 | 4.73 | 2.95 |
| 102.28 | 0.3345 | 1.7e7 | 260.06 | 4.72 | 2.94 |
| 102.28 | 0.3344 | 1.9e7 | 260.08 | 4.71 | 2.94 |
| 98.23 | 0.3343 | 4.1e6 | 260.09 | 4.52 | 2.82 |
| 98.23 | 0.3352 | 5.6e6 | 259.95 | 4.57 | 2.86 |
| 98.23 | 0.3346 | 4.7e6 | 260.05 | 4.53 | 2.83 |
| 94.34 | 0.3347 | 8.4e5 | 260.03 | 4.36 | 2.72 |
| 94.34 | 0.3349 | 9.6e5 | 259.99 | 4.37 | 2.73 |
| 94.34 | 0.3347 | 7.0e5 | 260.02 | 4.36 | 2.72 |

E. $T_0=32.45$ °C $\omega_1=1.2621\%$ $\omega_2=0.05346\%$ $x=0.492$

| $p_0$ | $\Delta p/p_0$ | $J_{\exp t}$ | $T_{\exp t}$ | $a_1$ | $a_2$ |
|---|---|---|---|---|---|
| 113.15 | 0.3350 | 7.0e8 | 259.98 | 4.34 | 4.20 |
| 113.15 | 0.3351 | 7.3e8 | 259.96 | 4.34 | 4.20 |
| 113.15 | 0.3348 | 7.1e8 | 260.00 | 4.33 | 4.19 |
| 108.67 | 0.3346 | 2.0e8 | 260.03 | 4.15 | 4.01 |
| 108.67 | 0.3347 | 2.0e8 | 260.02 | 4.15 | 4.02 |
| 108.67 | 0.3346 | 2.0e8 | 260.04 | 4.15 | 4.01 |
| 104.37 | 0.3347 | 6.4e7 | 260.02 | 3.99 | 3.85 |
| 104.37 | 0.3349 | 6.3e7 | 260.00 | 4.00 | 3.86 |
| 104.37 | 0.3347 | 5.4e7 | 260.03 | 3.99 | 3.85 |
| 100.24 | 0.3347 | 1.4e7 | 260.03 | 3.83 | 3.70 |
| 100.24 | 0.3346 | 1.3e7 | 260.03 | 3.83 | 3.70 |
| 100.24 | 0.3344 | 1.4e7 | 260.07 | 3.82 | 3.69 |
| 92.27 | 0.3345 | 2.0e6 | 260.05 | 3.67 | 3.55 |
| 96.27 | 0.3346 | 2.6e6 | 260.03 | 3.68 | 3.55 |
| 96.27 | 0.3346 | 3.3e6 | 260.04 | 3.67 | 3.55 |
| 92.46 | 0.3342 | 5.9e5 | 260.11 | 3.51 | 3.39 |
| 92.46 | 0.3344 | 8.4e5 | 260.07 | 3.52 | 3.40 |
| 92.46 | 0.3347 | 7.9e5 | 260.02 | 3.53 | 3.41 |

F. $T_0=32.49$ °C $\omega_1=1.0147\%$ $\omega_2=0.06446\%$ $x=0.592$

| $p_0$ | $\Delta p/p_0$ | $J_{\exp t}$ | $T_{\exp t}$ | $a_1$ | $a_2$ |
|---|---|---|---|---|---|
| 113.15 | 0.3349 | 3.3e8 | 259.99 | 3.48 | 5.04 |
| 113.15 | 0.3348 | 3.6e8 | 259.99 | 3.48 | 5.04 |
| 113.15 | 0.3351 | 3.9e8 | 259.95 | 3.49 | 5.06 |
| 108.67 | 0.3348 | 1.0e8 | 260.00 | 3.34 | 4.84 |
| 108.67 | 0.3347 | 1.1e8 | 260.01 | 3.33 | 4.83 |
| 108.67 | 0.3347 | 1.1e8 | 260.01 | 3.33 | 4.83 |
| 104.37 | 0.3346 | 3.2e7 | 260.03 | 3.20 | 4.63 |
| 104.37 | 0.3349 | 2.5e7 | 259.98 | 3.21 | 4.66 |
| 104.37 | 0.3347 | 2.4e7 | 260.01 | 3.20 | 4.64 |
| 100.24 | 0.3346 | 5.2e6 | 260.03 | 3.07 | 4.45 |
| 100.24 | 0.3349 | 6.5e6 | 259.99 | 3.08 | 4.47 |
| 100.24 | 0.3348 | 5.0e6 | 260.00 | 3.08 | 4.46 |
| 96.27 | 0.3346 | 8.8e5 | 260.03 | 2.95 | 4.27 |
| 96.27 | 0.3346 | 7.9e5 | 260.02 | 2.95 | 4.28 |
| 96.27 | 0.3347 | 1.0e6 | 260.01 | 2.95 | 4.28 |

G. $T_0=32.52$ °C $\omega_1=0.8155\%$ $\omega_2=0.07791\%$ $x=0.685$

| $p_0$ | $\Delta p/p_0$ | $J_{\exp t}$ | $T_{\exp t}$ | $a_1$ | $a_2$ |
|---|---|---|---|---|---|
| 113.15 | 0.3347 | 4.7e8 | 260.01 | 2.79 | 6.07 |
| 113.15 | 0.3347 | 4.8e8 | 260.01 | 2.79 | 6.07 |
| 113.15 | 0.3349 | 4.9e8 | 259.98 | 2.79 | 6.09 |
| 108.67 | 0.3350 | 1.4e8 | 259.96 | 2.68 | 5.86 |
| 108.67 | 0.3347 | 1.1e8 | 260.00 | 2.68 | 5.83 |
| 108.67 | 0.3348 | 1.0e8 | 260.00 | 2.68 | 5.84 |
| 104.37 | 0.3345 | 2.6e7 | 260.05 | 2.56 | 5.58 |
| 104.37 | 0.3349 | 2.4e7 | 259.98 | 2.57 | 5.62 |
| 104.37 | 0.3346 | 2.3e7 | 260.02 | 2.57 | 5.59 |

TABLE I. (*Continued*.)

| | | | | | |
|---|---|---|---|---|---|
| G. $T_0=32.52$ °C $\omega_1=0.8155\%$ $\omega_2=0.07791\%$ $x=0.685$ | | | | | |
| 100.24 | 0.3347 | 4.7*e*6 | 260.01 | 2.47 | 5.38 |
| 100.24 | 0.3348 | 5.2*e*6 | 259.99 | 2.47 | 5.39 |
| 100.24 | 0.3348 | 5.1*e*6 | 260.00 | 2.47 | 5.38 |
| 96.27 | 0.3345 | 8.6*e*5 | 260.03 | 2.37 | 5.15 |
| 96.27 | 0.3347 | 9.6*e*5 | 260.01 | 2.37 | 5.17 |
| 96.27 | 0.3346 | 7.2*e*5 | 260.03 | 2.37 | 5.16 |
| H. $T_0=32.55$ °C $\omega_1=0.6155\%$ $\omega_2=0.09192\%$ $x=0.773$ | | | | | |
| $p_0$ | $\Delta p/p_0$ | $J_{exp\,t}$ | $T_{exp\,t}$ | $a_1$ | $a_2$ |
| 115.46 | 0.3350 | 3.3*e*8 | 259.96 | 2.15 | 7.33 |
| 115.46 | 0.3351 | 4.3*e*8 | 259.94 | 2.15 | 7.34 |
| 115.46 | 0.3350 | 3.3*e*8 | 259.96 | 2.15 | 7.33 |
| 115.46 | 0.3351 | 4.8*e*8 | 259.95 | 2.15 | 7.34 |
| 115.46 | 0.3350 | 4.7*e*8 | 259.96 | 2.15 | 7.33 |
| 115.46 | 0.3349 | 4.9*e*8 | 259.98 | 2.15 | 7.32 |
| 110.89 | 0.3347 | 1.1*e*8 | 260.00 | 2.06 | 7.01 |
| 110.89 | 0.3349 | 9.7*e*7 | 259.97 | 2.06 | 7.03 |
| 110.89 | 0.3347 | 1.1*e*8 | 260.00 | 2.06 | 7.01 |
| 106.50 | 0.3351 | 1.8*e*7 | 259.95 | 1.98 | 6.77 |
| 106.50 | 0.3348 | 1.7*e*7 | 260.00 | 1.98 | 6.74 |
| 106.50 | 0.3348 | 1.7*e*7 | 259.99 | 1.98 | 6.74 |
| 102.28 | 0.3345 | 2.6*e*6 | 260.03 | 1.89 | 6.45 |
| 102.28 | 0.3345 | 2.5*e*6 | 260.04 | 1.89 | 6.44 |
| 102.28 | 0.3345 | 2.2*e*6 | 260.03 | 1.89 | 6.45 |
| 102.28 | 0.3348 | 1.9*e*6 | 259.99 | 1.90 | 6.48 |
| 98.23 | 0.3346 | 5.8*e*5 | 260.02 | 1.82 | 6.20 |
| 98.23 | 0.3348 | 4.2*e*5 | 260.00 | 1.82 | 6.22 |
| 98.23 | 0.3347 | 3.9*e*5 | 260.01 | 1.82 | 6.21 |
| I. $T_0=32.57$ °C $\omega_1=0.4750\%$ $\omega_2=0.1162\%$ $x=0.848$ | | | | | |
| $p_0$ | $\Delta p/p_0$ | $J_{exp\,t}$ | $T_{exp\,t}$ | $a_1$ | $a_2$ |
| 110.89 | 0.3348 | 5.4*e*8 | 260.00 | 1.59 | 8.85 |
| 110.89 | 0.3349 | 5.3*e*8 | 260.00 | 1.59 | 8.85 |
| 110.89 | 0.3349 | 5.2*e*8 | 260.00 | 1.59 | 8.85 |
| 106.50 | 0.3347 | 7.9*e*7 | 260.03 | 1.52 | 8.48 |
| 106.50 | 0.3347 | 9.4*e*7 | 260.03 | 1.52 | 8.48 |
| 106.50 | 0.3349 | 9.8*e*7 | 259.99 | 1.52 | 8.51 |
| 102.28 | 0.3346 | 1.6*e*7 | 260.03 | 1.46 | 8.14 |
| 102.28 | 0.3346 | 1.2*e*7 | 260.05 | 1.46 | 8.13 |
| 102.28 | 0.3347 | 1.1*e*7 | 260.02 | 1.46 | 8.15 |
| 102.28 | 0.3348 | 1.4*e*7 | 260.01 | 1.46 | 8.16 |
| 98.23 | 0.3347 | 2.2*e*6 | 260.03 | 1.40 | 7.82 |
| 98.23 | 0.3345 | 1.8*e*6 | 260.06 | 1.40 | 7.80 |
| 98.23 | 0.3347 | 1.7*e*6 | 260.02 | 1.40 | 7.82 |
| 94.34 | 0.3346 | 3.6*e*5 | 260.05 | 1.34 | 7.50 |
| 94.34 | 0.3346 | 2.6*e*5 | 260.04 | 1.35 | 7.50 |
| 94.34 | 0.3348 | 4.6*e*5 | 260.01 | 1.35 | 7.52 |
| 94.34 | 0.3347 | 2.8*e*5 | 260.02 | 1.35 | 7.52 |
| J. $T_0=32.59$ °C $\omega_1=0.2365\%$ $\omega_2=0.1368\%$ $x=0.929$ | | | | | |
| $p_0$ | $\Delta p/p_0$ | $J_{exp\,t}$ | $T_{exp\,t}$ | $a_1$ | $a_2$ |
| 117.82 | 0.3349 | 7.6*e*8 | 259.99 | 0.84 | 11.07 |
| 117.82 | 0.3348 | 7.3*e*8 | 260.00 | 0.84 | 11.05 |
| 113.15 | 0.3346 | 1.8*e*8 | 260.03 | 0.80 | 10.58 |
| 113.15 | 0.3348 | 1.4*e*8 | 260.00 | 0.80 | 10.62 |
| 113.15 | 0.3351 | 1.7*e*8 | 259.96 | 0.81 | 10.66 |
| 108.67 | 0.3346 | 2.9*e*7 | 260.03 | 0.77 | 10.16 |
| 108.67 | 0.3348 | 2.5*e*7 | 260.00 | 0.77 | 10.19 |
| 104.37 | 0.3346 | 5.5*e*6 | 260.03 | 0.74 | 9.77 |
| 104.37 | 0.3347 | 4.2*e*6 | 260.01 | 0.74 | 9.78 |
| 104.37 | 0.3349 | 4.6*e*6 | 259.98 | 0.74 | 9.82 |
| 100.24 | 0.3346 | 8.6*e*5 | 260.03 | 0.71 | 9.38 |
| 100.24 | 0.3343 | 7.0*e*5 | 260.08 | 0.71 | 9.33 |
| 100.24 | 0.3348 | 8.2*e*5 | 260.00 | 0.71 | 9.41 |

TABLE I. (*Continued*.)

| | | | | | |
|---|---|---|---|---|---|
| K. $T_0=32.60$ °C $\omega_1=0\%$ $\omega_2=0.1502\%$ $x=1$ | | | | | |
| $p_0$ | $\Delta p/p_0$ | $J_{exp\,t}$ | $T_{exp\,t}$ | $a_1$ | $a_2$ |
| 122.67 | 0.3348 | 5.4*e*8 | 259.98 | 0 | 12.64 |
| 122.67 | 0.3348 | 6.7*e*8 | 259.98 | 0 | 12.64 |
| 122.67 | 0.3346 | 6.2*e*8 | 260.00 | 0 | 12.61 |
| 117.81 | 0.3345 | 1.7*e*8 | 260.02 | 0 | 12.08 |
| 117.81 | 0.3344 | 1.6*e*8 | 260.03 | 0 | 12.07 |
| 113.14 | 0.3341 | 3.3*e*7 | 260.07 | 0 | 11.55 |
| 113.14 | 0.3344 | 3.3*e*7 | 260.04 | 0 | 11.59 |
| 113.14 | 0.3344 | 2.9*e*7 | 260.02 | 0 | 11.60 |
| 108.66 | 0.3343 | 8.9*e*6 | 260.05 | 0 | 11.12 |
| 108.66 | 0.3341 | 4.3*e*6 | 260.08 | 0 | 11.08 |
| 108.66 | 0.3345 | 7.8*e*6 | 260.02 | 0 | 11.15 |
| 104.36 | 0.3343 | 1.5*e*6 | 260.05 | 0 | 10.67 |
| 104.36 | 0.3345 | 1.3*e*6 | 260.01 | 0 | 10.71 |
| 104.36 | 0.3344 | 1.4*e*6 | 260.02 | 0 | 10.70 |
| 102.27 | 0.3344 | 4.8*e*5 | 260.03 | 0 | 10.48 |
| 102.27 | 0.3344 | 3.4*e*5 | 260.03 | 0 | 10.48 |
| 102.27 | 0.3343 | 5.0*e*5 | 260.05 | 0 | 10.46 |

The intersection of the nucleation rate surface and the $a_1$-$a_2$ plane at $J_0=10^7$ cm$^{-3}$ s$^{-1}$ is shown for water-*n*-pentanol in Fig. 4, curve $i=5$. The full triangles in Fig. 4 actually indicate the onset activities $a_{10}$ and $a_{20}$ for water-*n*-pentanol corresponding to the reference nucleation rate $J_0$. These onset activities are determined with comparatively high accuracy from the best fits to the individual nucleation rate curves as shown in Fig. 2.

As can be seen from Fig. 4, water and *n*-pentanol support each other in the nucleation process stronger than ideal mixtures. This can be judged from the fact that nucleation occurs at lower activities than expected for a linear combi-

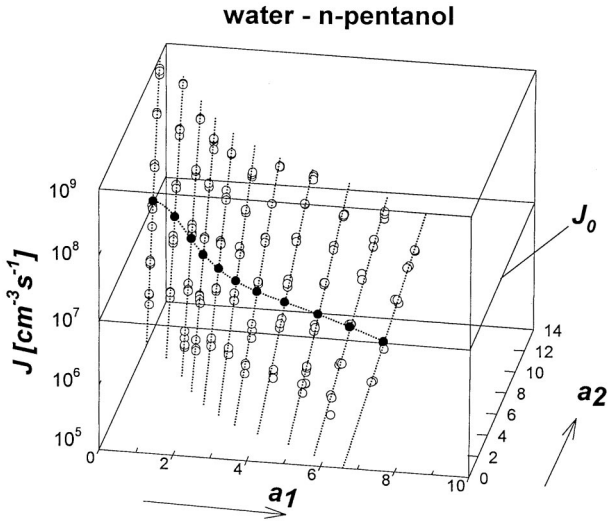


FIG. 3. Three-dimensional representation of the data (open points) of Fig. 2 shaping a nucleation rate surface $J(a_1,a_2)$. The intersection of this surface which with a plane at constant nucleation rate $J_0=10^7$ cm$^{-3}$ s$^{-1}$ yields the corresponding onset activities (full points). The line connecting the full points is a 6th-order polynomial providing $da_2/da_1$ at each point.

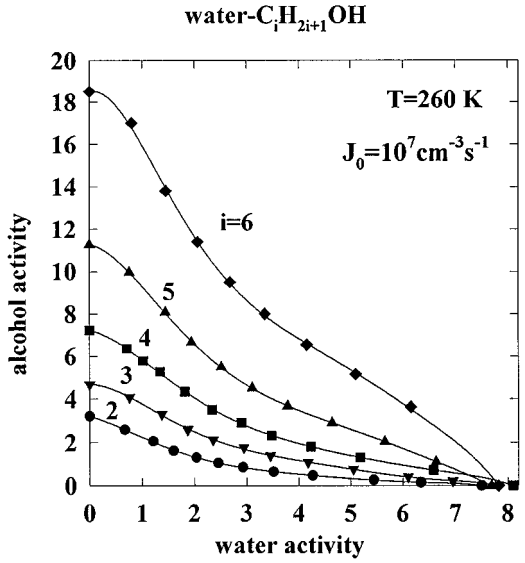


FIG. 4. Onset activities corresponding to the reference nucleation rate $J_0=10^7$ cm$^{-3}$ s$^{-1}$ for the water-*n*-alcohol systems ranging from ethanol ($i=2$) to *n*-hexanol ($i=6$). Note the homologous trend. The full triangles correspond to the full points in Fig. 3.

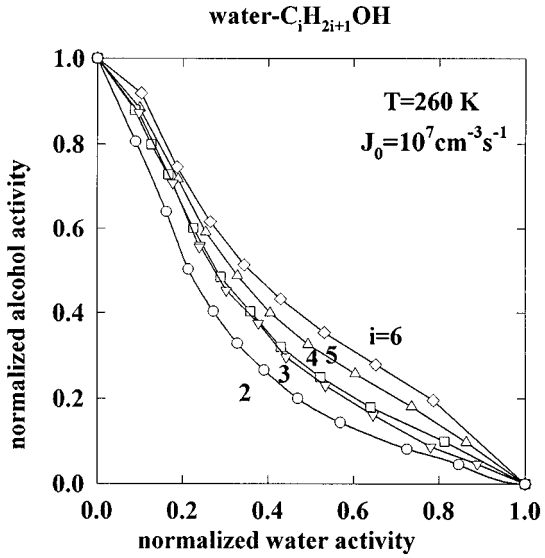


FIG. 5. Onset activities shown in Fig. 4 normalized by the activities of pure water and pure alcohol systems [Eq. (10)]. The symbols correspond to those of Fig. 4. Note the decreasing mutual nucleation enhancement with increasing alcohol chain length $i$.

nation of the onset activities $a_{10}^0$ and $a_{20}^0$ for the *pure* components corresponding to a straight line connecting the onset activities of the pure components. The deviation is apparently largest for intermediate activity fractions.

The smooth curves through the data points in Fig. 4 correspond to 6th-order polynomials, which serve to accurately determine the slopes $\partial a_2/\partial a_1$ at fixed reference nucleation rate $J_0$. As mentioned in the theoretical sections of papers I and II,[29,30] the slopes $\partial \ln J/\partial a$ at fixed activity fraction $x$ as obtained from the $\ln J$ versus $a$ curves in Fig. 2 together with the slopes $\partial a_2/\partial a_1$ at fixed $J_0$, as obtained from the $a_{20}$ versus $a_{10}$ curves in Fig. 4 suffice to determine the number of molecules in the critical cluster. This will be further discussed in the next section.

The onset activities for the other water-*n*-alcohol systems considered in the present study are indicated in Fig. 4 as well. A systematic trend of the onset activities of the alcohols with increasing molecular chain length toward higher activities is observed. The shape of the $a_{20}$ versus $a_{10}$ curves, however, remains similar. In particular, no indication of phase separation is found for the three higher alcohols, although macroscopic miscibility gaps occur in these systems.

In order to demonstrate the systematic change in the nucleation behavior with varying alkyl chain length, it is useful to consider normalized vapor phase activities

$$a_{i,\mathrm{norm}}=\frac{a_i}{a_{i0}^0}, \quad (i=1,2) \tag{10}$$

of the vapors considered, where $a_{10}^0$ and $a_{20}^0$ are the onset activities for the corresponding *pure* vapors, respectively. Correspondingly we introduce the normalized activity fraction

$$x_{\mathrm{norm}}=\frac{a_{2,\mathrm{norm}}}{a_{1,\mathrm{norm}}+a_{2,\mathrm{norm}}} \tag{11}$$

of the alcohol considered. Figure 5 shows the normalized onset activities $a_{10,\mathrm{norm}}$ and $a_{20,\mathrm{norm}}$ corresponding to the reference nucleation rate $J_0$ for the water-*n*-alcohol systems considered.

It can be seen from Fig. 5 that the mutual enhancement of nucleation seen most clearly for water-ethanol is apparently reduced with increasing alkyl chain length of the alcohol. This might actually have been expected in view of the increasing miscibility gap occurring for the higher alcohols.

### C. Measurement of molecular content of nuclei

The numbers of molecules in the critical clusters can without reference to any specific nucleation theory be obtained to a good approximation from the slopes of the nucleation rate surface.[26–31] As described above, our measurements allow the quantitative determination of the nucleation rate surface in the $\ln J-a_1-a_2$ space for a fixed temperature $T$. Aside from the respective onset activities $a_{10}$ and $a_{20}$ corresponding to the reference nucleation rate $J_0$, the determination of the slopes of the experimentally determined nucleation rate surface only requires the knowledge of $\partial \ln J/\partial a$ at fixed activity fraction $x$ and $\partial a_2/\partial a_1$ at fixed reference nucleation rate $J_0$.[29] The former is the slope of the respective steep dotted line in Fig. 3, whereas the latter is the derivative of the dotted line in the plane corresponding to the reference nucleation rate $J_0=10^7$ cm$^{-3}$ s$^{-1}$ in Fig. 3. Both of these derivatives can be determined quite accurately from proper numerical fits to the corresponding experimental data. The slopes of the nucleation rate surface and thus the numbers $n_1^*$ and $n_2^*$ of the respective molecules in the critical clusters are expressed as[29]

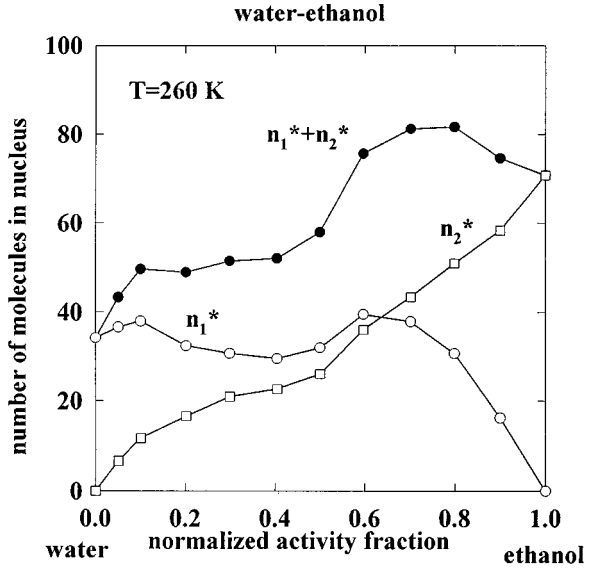


FIG. 6. Molecular content of the critical nuclei as function of normalized activity fraction [vapor composition, Eq. (11)] for water-ethanol. $n_1^*$ and $n_2^*$ are the numbers of water and ethanol molecules in the critical nucleus, respectively. Note the enrichment of the clusters with ethanol on the water side and with water on the ethanol side.

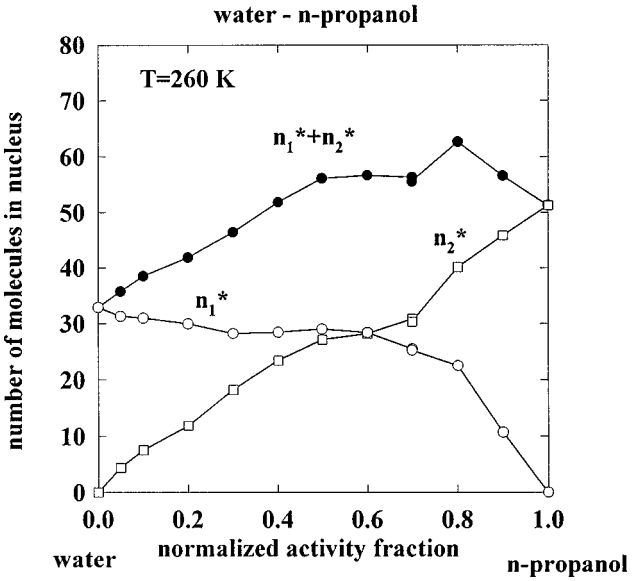


FIG. 7. As Fig. 6, for water-*n*-propanol.

$$n_1^* \approx \left.\frac{\partial \ln J}{\partial \ln a_1}\right|_{a_2} = -a_{10}\left.\frac{\partial a_2}{\partial a_1}\right|_{J_0}\left.\frac{\partial \ln J}{\partial a}\right|_x \times\left[1+\left(\frac{a_{20}}{a_{10}}\right)^2\right]^{1/2}\left[\frac{a_{20}}{a_{10}}-\left.\frac{\partial a_2}{\partial a_1}\right|_{J_0}\right]^{-1}, \tag{12}$$

$$n_2^* \approx \left.\frac{\partial \ln J}{\partial \ln a_2}\right|_{a_1} = a_{20}\left.\frac{\partial \ln J}{\partial a}\right|_x\left[1+\left(\frac{a_{20}}{a_{10}}\right)^2\right]^{1/2} \times\left[\frac{a_{20}}{a_{10}}-\left.\frac{\partial a_2}{\partial a_1}\right|_{J_0}\right]^{-1}. \tag{13}$$

In Figs. 6 to 10 the numbers $n_1^*$ and $n_2^*$ of molecules in the critical clusters are shown for all systems studied.

A quite similar shape of the curves is observed for all systems. For the water-*n*-pentanol system presented here in detail the measured numbers of water molecules $n_1^*$, *n*-pentanol molecules $n_2^*$, as well as the total number of molecules $n_1^* + n_2^*$ in the critical clusters, are shown in Fig. 9 as function of the normalized activity fraction $x_{\text{norm}}$ of *n*-pentanol. Considering the *normalized* activity fraction allows to present the data as evenly spaced points in the figures. As can be seen, aside from experimental scatter, the number of water molecules $n_1^*$ in the nuclei remains quite high until $x_{\text{norm}}=0.8$ and it even exhibits a slight maximum. The number of *n*-pentanol molecules $n_2^*$ increases monotonically, but shows an enrichment of *n*-pentanol at very low alcohol activities. These are typical observations for all alcohols considered (see Figs. 6 to 10). In each case the number of water molecules remains quite high, while the alcohol molecules enrich in the clusters at low activity fractions.

For quantitative comparison of the different systems the average mole fraction

$$x_{\text{av}}^* = \frac{n_2^*}{n_1^*+n_2^*} \tag{14}$$

of alcohol in the critical clusters may be considered. In this connection it should be noted that significant spacial nonuniformities of the critical clusters can be expected, particularly for nonideal systems. According to the theoretical treatment in the preceding papers,[29,30] as well as from the thermodynamic derivation by Oxtoby and Kashchiev,[31] it is clear,

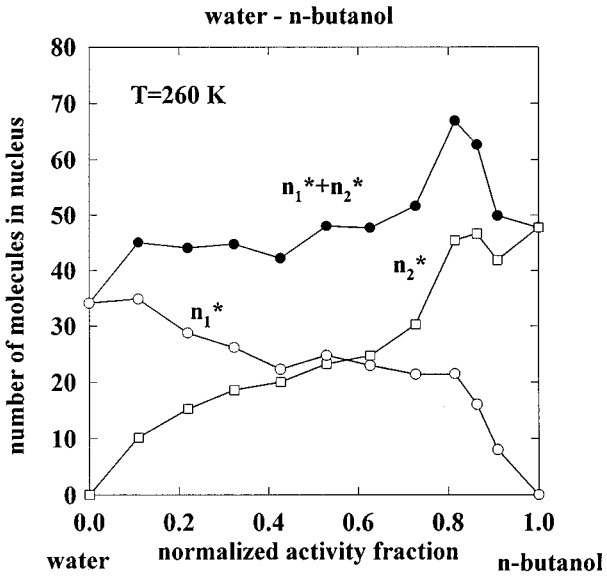


FIG. 8. As Fig. 6, for water-*n*-butanol.

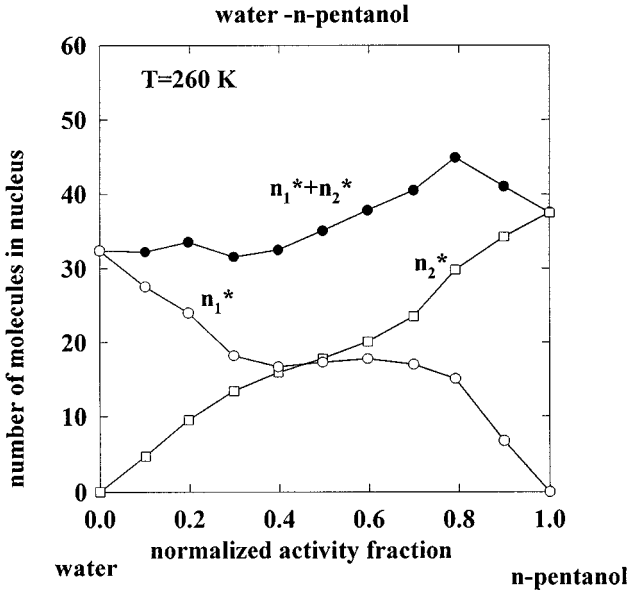


FIG. 9. As Fig. 6, for water-*n*-pentanol.

however, that the determination of the number of each type of molecules in the critical clusters from the slopes of the nucleation rate surface is insensitive to and independent of the actual structure of the clusters. A comparison of the average mole fractions $x_{av}^*$ is presented in Fig. 11.

A quite similar behavior of all systems considered is observed. As can be seen the alcohols are enriched already for low alcohol activity fractions. On the other hand also water is enriched for low water activity fractions. Therefore, the average mole fractions $x_{av}^*$ of the critical nuclei shape sigmoidal curves deviating systematically from an ideal case of identical molecules that would correspond to the dashed line in Fig. 11.

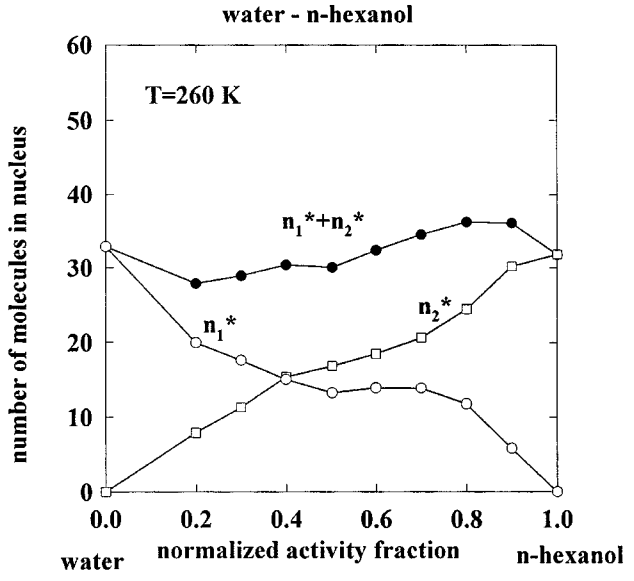


FIG. 10. As Fig. 6, for water-*n*-hexanol.

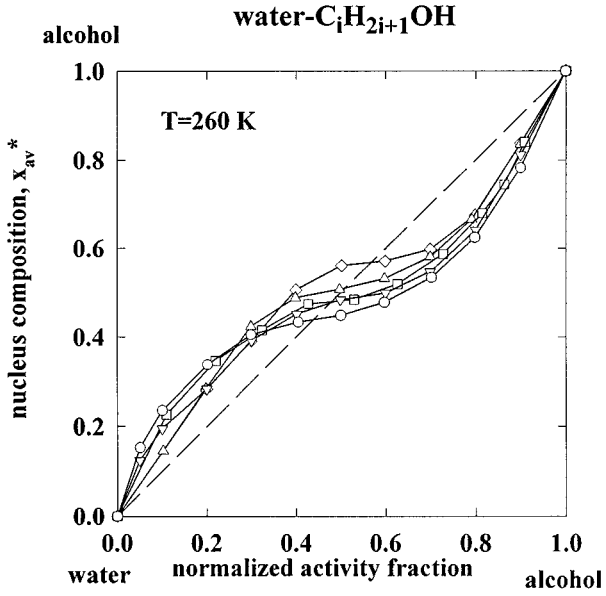


FIG. 11. Average compositions of critical nuclei, $x_{av}^*$ as function of normalized activity fraction where $x_{av}^* = n_2^*/(n_1^* + n_2^*)$. The symbols correspond to those of Figs. 4 and 5. The ideal case of identical molecules is indicated as straight dashed line. Note the enrichment of the nuclei with alcohol on the water side and with water on the alcohol side for all systems.

## IV. DISCUSSION

### A. Molecular content of unary nuclei

The measured numbers $n^*$ of molecules in the critical clusters for the six unary systems considered, namely water and the five *n*-alcohols $C_iH_{2i+1}OH$ ($i=2,\ldots,6$) are indicated as function of the carbon chain number $i$ by the full circles in Fig. 12. Note that water can formally be considered as the compound with carbon chain number $i=0$ in the homolo-

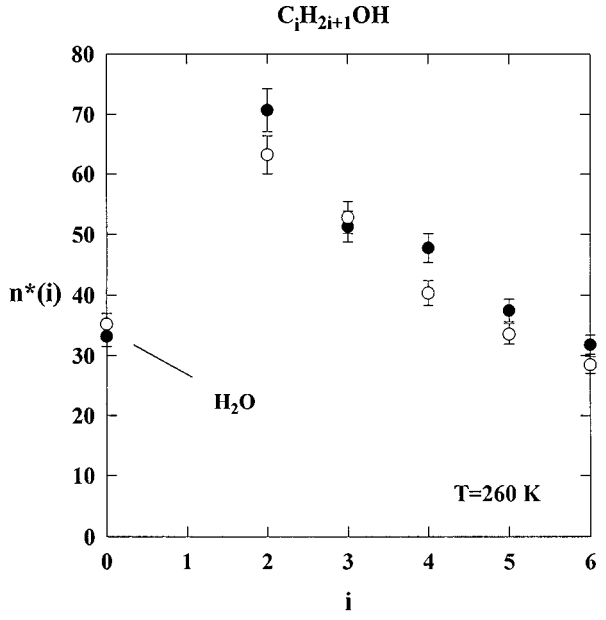


FIG. 12. Measured molecular content for pure water and the pure alcohols $C_iH_{2+1}OH$ (full symbols). The predicted numbers according to the Gibbs–Thomson equation [Eq. (15)] are shown for comparison (open symbols).

gous series of $n$-alcohols and may therefore be represented together with the $n$-alcohols in the same graph. It should be mentioned that the hydrocarbon chain is crucial for the alcohol to act as an amphiphile. In a forthcoming paper on the binary $n$-nonane-$n$-alcohol systems we shall show that in this connection water actually appears to behave as the first homologue in the $C_iH_{2i+1}OH$ series.

For comparison the numbers of molecules in the unary critical clusters were also calculated according to the Gibbs–Thomson equation

$$n^* = \frac{4\pi r^{*3}}{3\nu_m} = \frac{32\pi\sigma^3\nu_m^2}{3(kT\ln a_0)^3}, \tag{15}$$

where $r^*$ is the corresponding radius of the unary critical cluster and $a_0$ is the respective onset activity (supersaturation) of the unary vapor considered. $\nu_m$ and $\sigma$ denote the *macroscopic* values of molecular volume and surface tension of the condensing unary liquid, respectively. In the calculations for alcohols we used the surface tensions measured by Strey and Schmeling,[63] the densities compiled in the same paper, and the equilibrium vapor pressures measured by Schmeling and Strey.[64] For water we used the parameters given by Viisanen *et al.*[28] The predictions by the Gibbs–Thomson equation are indicated as open circles in Fig. 12 showing quite good agreement with the corresponding experimental data for all compounds considered. The overall agreement will even be improved considering that the experimental $n^*$ contain a small contribution amounting to about 1 or 2 molecules from the variation of the prefactor $K$.[26,29] It surprises how accurately the macroscopic droplet model is accounting for the properties of microscopic clusters containing only 30 to 70 molecules, particularly in view of the fact that macroscopic parameters are used in the calculation. The quantitative agreement shown in Fig. 12 is consistent with the qualitative observation that the slopes of experimental nucleation rate versus supersaturation curves are often correctly predicted by the classical nucleation theory even if the actual values of the nucleation rates are differing by several orders of magnitude.[35,36,48,65]

### B. Molecular content of binary nuclei

Considering the series of five binary systems shown in Figs. 6 to 10 one finds quite similar behavior. An at first sight somewhat unexpected feature is the enrichment of the alcohol clusters with water. Checking macroscopic water-$C_iH_{2+1}OH$ phase diagrams for $i>3$ one finds that there is approximately a 20 wt % solubility of water in alcohols nearly independent of $i$. In terms of mole fractions this means that for mole fractions of water up to about 0.3 there is no phase separation to be expected.

For each system there is a maximum or hump of the $n_1^*$ curve on the alcohol side. Considering the water side of the $n_1^*$ curves we observe that for the short chain alcohols the $n_1^*$ are located above a straight line connecting the $n_1^*$ of pure water with zero for $x_{\text{norm}}=1$. The opposite is true for the long chain alcohols. The corresponding crossover is observed between $n$-propanol and $n$-butanol, those compounds in the homologous series, where the macroscopic phase behavior changes from miscible to partially miscible.

Performing the analogous considerations for the $n_2^*$ curves on finds on the water-rich side an enrichment of the clusters with alcohol for all systems. This enrichment was not unexpected, because alcohols are surface active and lower the surface tensions which in turn makes nucleation easier. However, the enrichment decreases with increasing alcohol chain length. At closer consideration also this trend appears plausible, if one conceives the cluster to be divided into bulk and surface regions: As the chain length of the alcohol increases, even at constant surface activity, the increasing tendency of hydrocarbon chain incompatibility with water (the hydrophobic effect[66]) could lead to a depletion of the interior of the water-rich cluster. Macroscopically, the solubility of alcohols drops from about 7 wt % for $n$-butanol to 1 wt % for $n$-hexanol. Therefore, the overall number of alcohol molecules in the clusters is expected to decrease.

The above described enrichments with water and with alcohol are clearly observed by considering the average mole fractions of the critical clusters as shown in Fig. 11. Furthermore it can be seen from Fig. 11 that critical clusters with average compositions ranging continuously from pure water to pure alcohol were found for all alcohols considered. This is particularly notable for the higher alcohols, where macroscopic phase separation is expected for mole fractions of alcohol between about 0.1 and 0.7. Apparently binary water-alcohol microclusters are forming regardless of macroscopic phase separation. In this connection it should be noted, however, that the data on macroscopic solubility refer to bulk properties of the systems considered. Due to possible enrichment effects at the surface of the small critical clusters their average mole fractions $x_{\text{av}}^*$ may not be directly comparable to the corresponding bulk properties available from macroscopic measurements.

For the water-ethanol system we demonstrated in the preceding paper II[30] that the essential features of the experimental $n_1^*$, $n_2^*$, and $n_1^* + n_2^*$ curves are surprisingly well accounted for by a simple cluster model.[30] The idea of Mirabel and co-workers[17] to apply the Guggenheim treatment of the planar water-ethanol surface tension[62] to calculate the surface energy of small clusters was further developed by Laaksonen and Kulmala.[18,19] A generalization to the case of partially miscible binary systems is the next step. However, one will have to develop a tractable way of treating the region of partial miscibility for which neither surface tension nor equilibrium vapor pressures can be measured.

It has been recognized before[12,16,30,61] that the classical theory of binary homogeneous nucleation fails to describe the nucleation behavior for nonideal mixtures. Moreover, at present there is apparently no theory available, which allows a thermodynamically consistent treatment of homogeneous nucleation of partially miscible liquids. Accordingly, at this point we have no theory which would allow a quantitative prediction of our experimental results. A theoretical description of homogeneous nucleation for systems which show nonideal behavior or partial miscibility is urgently needed in

TABLE II. Onset activities for water ($a_{10}$)-*n*-alcohol ($a_{20}$) systems for $T=260$ K. The corresponding molecular content $n_1^*$ and $n_2^*$ of the critical clusters according to Eqs. 12 and 13 are also given.

| $a_{10}$ | $a_{20}$ | $n_1^*$ | $n_2^*$ |
|---|---|---|---|
| | A. water-ethanol | | |
| 0.00 | 3.20 | 0 | 70.7 |
| 0.67 | 2.58 | 16.2 | 58.3 |
| 1.21 | 2.05 | 30.6 | 51.0 |
| 1.60 | 1.61 | 37.8 | 43.3 |
| 2.04 | 1.29 | 39.5 | 36.1 |
| 2.46 | 1.05 | 32.0 | 26.0 |
| 2.93 | 0.85 | 29.5 | 22.6 |
| 3.52 | 0.64 | 30.6 | 20.9 |
| 4.27 | 0.46 | 32.4 | 16.5 |
| 5.44 | 0.26 | 37.9 | 11.7 |
| 6.34 | 0.14 | 36.7 | 6.6 |
| 7.50 | 0.00 | 34.2 | 0 |
| | B. water-*n*-propanol | | |
| $a_{10}$ | $a_{20}$ | $n_1^*$ | $n_2^*$ |
| 7.82 | 0.00 | 32.9 | 0 |
| 6.95 | 0.22 | 31.3 | 4.4 |
| 6.10 | 0.40 | 31.0 | 7.5 |
| 5.05 | 0.75 | 30.0 | 11.9 |
| 4.18 | 1.07 | 28.2 | 18.2 |
| 3.46 | 1.38 | 28.4 | 23.4 |
| 2.95 | 1.75 | 29.0 | 27.1 |
| 2.36 | 2.11 | 28.4 | 28.2 |
| 1.88 | 2.61 | 25.5 | 30.8 |
| 1.87 | 2.59 | 25.2 | 30.3 |
| 1.38 | 3.30 | 22.5 | 40.2 |
| 0.76 | 4.07 | 10.7 | 45.9 |
| 0.00 | 4.66 | 0 | 51.3 |
| | C. water-*n*-butanol | | |
| $a_{10}$ | $a_{20}$ | $n_1^*$ | $n_2^*$ |
| 8.10 | 0.00 | 34.1 | 0 |
| 6.58 | 0.72 | 34.8 | 10.2 |
| 5.18 | 1.30 | 28.8 | 15.3 |
| 4.23 | 1.80 | 26.2 | 18.6 |
| 3.48 | 2.31 | 22.2 | 20.0 |
| 2.90 | 2.91 | 24.8 | 23.2 |
| 2.34 | 3.50 | 22.9 | 24.7 |
| 1.82 | 4.34 | 21.4 | 30.3 |
| 1.34 | 5.26 | 21.5 | 45.5 |
| 1.02 | 5.77 | 16.5 | 46.7 |
| 0.71 | 6.35 | 8.0 | 41.9 |
| 0.00 | 7.22 | 0 | 47.8 |
| | D. water-*n*-pentanol | | |
| $a_{10}$ | $a_{20}$ | $n_1^*$ | $n_2^*$ |
| 7.68 | 0.00 | 32.4 | 0 |
| 6.63 | 1.10 | 27.5 | 4.7 |
| 5.65 | 2.04 | 24.0 | 9.5 |
| 4.64 | 2.90 | 18.2 | 13.4 |
| 3.79 | 3.67 | 16.6 | 15.8 |
| 3.11 | 4.50 | 17.3 | 17.8 |
| 2.52 | 5.49 | 17.7 | 20.1 |
| 1.95 | 6.66 | 17.0 | 23.5 |
| 1.45 | 8.08 | 15.0 | 29.8 |
| 0.76 | 9.96 | 6.8 | 34.3 |
| 0.00 | 11.3 | 0 | 37.5 |
| | E. water-*n*-hexanol | | |
| $a_{10}$ | $a_{20}$ | $n_1^*$ | $n_2^*$ |
| 7.82 | 0.00 | 32.9 | 0 |
| 6.15 | 3.62 | 20.0 | 7.9 |
| 5.10 | 5.15 | 17.6 | 11.3 |
| 4.16 | 6.54 | 15.0 | 15.4 |
| 3.36 | 8.00 | 13.2 | 16.9 |
| 2.69 | 9.50 | 13.9 | 18.5 |
| 2.07 | 11.4 | 13.9 | 20.6 |
| 1.46 | 13.8 | 11.7 | 24.5 |
| 0.80 | 17.0 | 5.8 | 30.2 |
| 0.00 | 18.5 | 0 | 31.8 |

view of various practical applications. Our data compiled in Table II should provide a useful basis for testing such a theory.

### C. Accuracy of the results

As has been discussed in more detail elsewhere,[28] errors of the experimental nucleation rates will not exceed a factor of 2. The calibration procedure for the piezoelectric pressure transducer involves comparison of the voltage from the charge amplifier to the reading of the Baratron pressure transducer on the time scale of seconds. As the pressure pulse is occurring on the time scale of milliseconds, an observed drift of the pressure signal in between these time ranges may lead to an inaccuracy of the temperature during nucleation of up to 1 K on absolute scale. We are presently examining this effect in more detail. It would result in a systematic decrease of the activities by a few percents, equivalent to an increase in nucleation rate by a factor of 2. This error, however, will not affect the comparison between the various systems considered, because all measurements reported would carry the same error. In this connection the essential feature is the reproducibility of the nucleation temperature, which is typically 0.05 K. The reproducibility of the whole set of nucleation rate curves may be judged from Table I. For each of the five binary systems one nucleation rate versus activity curve for pure water has been measured. The corresponding onset activities vary between 7.50 and 8.10 with an average of 7.78 and relative standard deviation of 0.028. The slopes of these five nucleation rate versus activity curves for pure water determine the number $n_1^*$ of water molecules in the critical nuclei. The corresponding experimental values of $n_1^*$ vary from 32.4 to 34.2 with an average of 33.3 and relative standard deviation of 0.024.

## V. CONCLUSIONS

A comprehensive set of data on homogeneous nucleation in water-*n*-alcohol vapor mixtures at fixed temperature has been obtained. Our measurements confirm and extend results so far available in the literature. Strong deviations from the behavior of ideal vapor mixtures were observed. Considering the onset activities in Fig. 4 we find that water and *n*-alcohols mutually enhance nucleation. However, this apparently happens irrespective of the alcohol chain length, which is somewhat surprising in view of the fact that water and the higher alcohols exhibit macroscopic miscibility gaps. Normalizing the onset activities in Fig. 5 reveals that the

mutual enhancement of binary nucleation of water and alcohol is somewhat reduced with increasing chain length of the alcohol. Apparently, the cluster geometry allows for an energetically favorable arrangement of otherwise only partially miscible molecules, water being expected to form mainly the interior of the clusters while alcohol molecules preferentially adsorb on the cluster surface. The consequences of this effect have been discussed in paper II[30] in terms of an explicit cluster model for water-ethanol[19] which showed remarkably close agreement with the experimental cluster composition. In Fig. 11 we have presented the cluster composition for five binary systems including the three higher alcohols which show macroscopic phase separation. Extension of the cluster model to those systems remains a theoretical challenge.

We want to emphasize that the classical droplet model does quite well for one-component liquid clusters as can also be seen from Fig. 12. It can be applied to the nucleation of fully miscible liquids as well, however, as it comes to account for nonideal behavior of binary systems it fails.[12,16,30,61] This then leads to useless predictions of nucleation rates for binary systems. The consequences for predictions of particle formation by nucleation in the atmosphere may be dramatic. Therefore a theory describing homogeneous nucleation for systems showing nonideal behavior or incomplete miscibility, is urgently needed. The individual numbers of molecules in the critical clusters presented in this paper should provide a body of data which could be used to test an improved nucleation theory.

We have shown how to obtain data on binary nucleation of water with miscible or partially miscible molecules, and we have shown how to extract the numbers of molecules forming the critical cluster, the crucial quantity in nucleation. In principle, there should be no additional complication if water is replaced by a hydrophobic substance, like *n*-nonane. Such studies will be reported in a forthcoming paper. Also the procedure worked out should be applicable to cases in which one component is a trace gas relevant for the atmosphere, like $NH_3$, $HNO_3$, and terpenes. Experimental nucleation studies for these systems are planned.

## ACKNOWLEDGMENT

The present work was performed in the department of Professor M. Kahlweit to whom we are indebted for continuous exchange of ideas and support.

[1] R. J. Charlson, J. E. Lovelock, M. D. Andrae, and S. G. Warren, Nature **326**, 655 (1987).
[2] C. R. T. Wilson, Philos. Trans. R. Soc. A, London **189**, 265 (1897).
[3] L. M. Russell, S. N. Pandis, and J. H. Seinfeld, J. Geophys. Res. **99**, 209 (1994).
[4] M. Volmer and A. Weber, Z. Phys. Chem. **125**, 236 (1926).
[5] R. Becker and W. Döring, Ann. Phys. **24**, 719 (1935).
[6] M. Volmer, *Kinetik der Phasenbildung* (Steinkopff, Dresden, 1939).
[7] See also W. Döring and K. Newmann, Z. Phys. Chem. A **186**, 14 (1940).
[8] H. Reiss, J. Chem. Phys. **18**, 840 (1950).
[9] G. J. Doyle, J. Chem. Phys. **35**, 795 (1961).
[10] R. G. Renninger, F. C. Hiller and R. C. Bone, J. Chem. Phys. **75**, 1584 (1981).
[11] G. Wilemski, J. Chem. Phys. **80**, 1370 (1984).
[12] G. Wilemski, J. Phys. Chem. **91**, 2492 (1987).
[13] G. Wilemski, J. Chem. Phys. **88**, 5134 (1988).
[14] P. Mirabel and J. L. Katz, J. Chem. Phys. **67**, 1697 (1977).
[15] P. Mirabel and H. Reiss, Langmuir **3**, 228 (1987).
[16] J. P. Garnier, P. Mirabel, and B. Migault, Chem. Phys. Lett. **115**, 101 (1985).
[17] C. Flageollet-Daniel, J. P. Garnier, and P. Mirabel, J. Chem. Phys. **78**, 2600 (1983).
[18] A. Laaksonen and M. Kulmala, J. Chem. Phys. **95**, 6745 (1991).
[19] A. Laaksonen, J. Chem. Phys. **97**, 1983 (1992).
[20] H. Reiss, J. L. Katz, and E. R. Cohen, J. Chem. Phys. **48**, 5553 (1968).
[21] H. Reiss, A. Tabzadeh, and J. Talbot, J. Chem. Phys. **92**, 1266 (1990).
[22] H. M. Ellerby, C. L. Weakliem, and H. Reiss, J. Chem. Phys. **95**, 9209 (1991).
[23] X. C. Zeng and D. W. Oxtoby, J. Chem. Phys. **95**, 5940 (1991).
[24] X. C. Zeng and D. W. Oxtoby, J. Chem. Phys. **94**, 4472 (1991).
[25] A. K. Ray, M. Chalam, and L. K. Peters, J. Chem. Phys. **85**, 2161 (1986).
[26] D. Kashchiev, J. Chem. Phys. **76**, 5098 (1982).
[27] D. Kashchiev, private communication, letter to R. Strey from Dec. 13, 1984.
[28] Y. Viisanen, R. Strey, and H. Reiss, J. Chem. Phys. **99**, 4680 (1993).
[29] R. Strey and Y. Viisanen, J. Chem. Phys. **99**, 4693 (1993).
[30] Y. Viisanen, R. Strey, A. Laaksonen, and M. Kulmala, J. Chem. Phys. **100**, 6062 (1994).
[31] D. W. Oxtoby and D. Kashchiev J. Chem. Phys. **100**, 7665 (1994).
[32] J. L. Katz and M. J. Ostermier, J. Chem. Phys. **47**, 478 (1967).
[33] J. L. Katz, J. Chem. Phys. **52**, 4733 (1970).
[34] R. Heist and H. Reiss, J. Chem. Phys. **59**, 665 (1973).
[35] A. Kacker and R. H. Heist, J. Chem. Phys. **82**, 2734 (1985).
[36] C. Hung, M. J. Kransnopoler, and J. L. Katz, J. Chem. Phys. **90**, 1856 (1989).
[37] M. P. Anisimov and A. G. Cherevko, J. Aerosol Sci. **16**, 97 (1985).
[38] B. E. Wyslouzil, J. H. Seinfeld, and R. C. Flagan, J. Chem. Phys. **94**, 6842 (1991).
[39] M. Volmer and H. Flood, Z. Phys. Chem. A **190**, 273 (1934).
[40] A. Sander and G. Damköhler, Naturwissenschaften **31**, 460 (1943).
[41] E. F. Allard and J. L. Kassner, Jr., J. Chem. Phys. **42**, 1401 (1965).
[42] R. Miller, R. J. Anderson, J. L. Kassner, and D. E. Hagen, J. Chem. Phys. **78**, 3204 (1983).
[43] J. L. Schmitt, Rev. Sci. Instrum. **52**, 1749 (1981).
[44] J. L. Schmitt, G. W. Adams, and R. A. Zalabsky, J. Chem. Phys. **77**, 2089 (1982).
[45] J. L. Schmitt, R. A. Zalabsky, and G. W. Adams, J. Chem. Phys. **79**, 4496 (1983).
[46] G. W. Adams, J. L. Schmitt, and R. A. Zalabsky, J. Chem. Phys. **81**, 5074 (1984).
[47] P. E. Wagner and R. Strey, J. Phys. Chem. **85**, 2694 (1981).
[48] P. E. Wagner and R. Strey, J. Chem. Phys. **80**, 5266 (1984).
[49] F. Peters and B. Paikert, Exp. Fluids **7**, 521 (1989).
[50] P. P. Wegener and B. J. C. Wu, in *Nucleation Phenomena*, edited by A. C. Zettlemoyer (Elsevier, Amsterdam, 1977), p. 325.
[51] M. B. Frish and G. Wilemski, in *Atmospheric Aerosols and Nucleation*, *Lecture Notes in Physics*, Vol. 309 (Springer, Berlin, 1988), p. 527.
[52] R. Strey, P. E. Wagner, and Y. Viisanen, J. Phys. Chem. **98**, 7748 (1994).
[53] F. Richarz, Ann. Phys. **19**, 639 (1906).
[54] P. E. Wagner, J. Colloid Interface Sci. **105**, 456 (1985).
[55] G. Mie, Ann. Phys. **25**, 377 (1908).
[56] M. Kerker, *The Scattering of Light* (Academic, New York, 1969).
[57] P. E. Wagner and R. Strey, in *Aerosols. Science, Industry, Health and Environment*, Vol. 1, edited by S. Masuda and K. Takahashi (Pergamon, New York, 1990), p. 201.
[58] S. Vietti and B. G. Schuster, J. Chem. Phys. **58**, 434 (1973).
[59] P. E. Wagner, J. Colloid Interface Sci. **44**, 181 (1973).
[60] R. Strey and P. E. Wagner, in *Atmospheric Aerosols and Nucleation*, *Lecture Notes in Physics*, Vol. 309 (Springer, Berlin, 1988), p. 111.
[61] R. Strey, P. E. Wagner, and Y. Viisanen in *Nucleation and Atmospheric Aerosols*, edited by N. Fukuta and P. E. Wagner (Deepak, Hampton, 1992), p. 111.
[62] E. A. Guggenheim, in *Thermodynamics* (North Holland, Amsterdam, 1967).
[63] R. Strey and T. Schmeling, Ber. Bunsenges. Phys. Chem. **87**, 324 (1983).
[64] T. Schmeling and R. Strey, Ber. Bunsenges. Phys. Chem. **87**, 871 (1983).
[65] R. Strey, P. E. Wagner, and T. Schmeling, J. Chem. Phys. **84**, 2325 (1986).
[66] C. Tanford, in *The Hydrophobic Effect* (Wiley, New York, 1973).